Supporting Information for

The Exploration of Crystallization Kinetics in Quasi Two-dimensional Perovskite and High Performance Solar Cells

Ning Zhou[a], Yiheng Shen[a], Liang Li[a], Shunquan Tan[a], Na Liu[b], Guanhaojie Zheng[a], Qi Chen[b], Huanping Zhou[a*]

a. Beijing Key Laboratory for Theory and Technology of Advanced Battery Materials, Department of Materials Science and Engineering, College of Engineering, Peking University No.5 Yiheyuan Road Haidian District, Beijing 100871, P. R. China

b. School of Materials Science and Engineering, Beijing Institute of Technology 5 Zhongguancun South Street, Beijing 100081, P. R. China

Experimental Section

Materials Preparation. MAI and FAI were synthesized using the methods reported everywhere. PbO (99.9%) were purchased from Macklin Corporation. HI aqueous solution (57% w/w) and H_3PO_2 aqueous solution (50% w/w) were purchased from Aladdin Industrial Corporation. Butyl amine and Poly (3, 4-ethylenedioxythiophene): poly (styrenesulfonate) (PEDOT:PSS), [6,6]-phenyl-C61-butyric acid methyl ester ($PC_{61}BM$) and bathocuproine (BCP) was purchased from Xi'an baolaite Technology Ltd. The raw Q-2D perovskite powders were prepared by combining PbO, MAI, FAI and BA in appropriate ratios in a HI/H_3PO_2 solvent mixture as described previously.[1]

Device fabrication. The inverted planar heterojunction PSCs were fabricated on ITO substrates. The ITO substrates were ultrasonically cleaned with diluted detergent, deionized water, acetone, ethanol

and isopropanol (IPA) in succession. The final perovskite powder dissolved in DMF at a concentration of 1mol/L. We fabricated the perovskite films by spin-coating the precursor solution on a cold tin indium oxide (ITO) glass substrates. The as-cleaned substrates were UV–ozone treated for 20 min. PEDOT:PSS solution was spin-coated onto the ITO substrates at 3000 rpm for 30 s, and the samples were then annealed at 120 °C for 20 min in air. The final perovskite powder dissolved in DMF at a concentration of 1mol/L. The perovskite precursor solution was spin-coated on the top of PEDOT:PSS modified ITO substrate at 2000 rpm for 30 s. The samples were further annealed on a hot plate at 70 °C for 20 min. Next, 30 μL of $PC_{61}BM$ (20 mg/mL in CB) solution was then spin-coated on the top of perovskite layer at 2000 rpm for 30 s and BCP (2.5 mg/mL in methanol) was dropped onto $PC_{61}BM$ at a rotational speed of 6000 rpm to form an electron extracting layer, and the samples were annealed on a hot plate at 70 °C for 10 min, respectively. Finally, 100 nm silver electrode was deposited via thermal evaporation under a pressure of 1×10^{-4} Pa. The active area was 0.102 cm^2.

Characterization. The XRD patterns were collected by using a PANalytical X'Pert Pro X-ray powder diffractometer with Cu Kα radiation (λ = 1.54050 Å). The morphology were measured using a scanning electron microscope (SEM) (S4800) and atomic force microscopy (Bruker). The Grazing incidence wide angle x-ray scattering (GIWAXS) data were obtained at beamline BL14B1 of the Shanghai Synchrotron Radiation Facility (SSRF) using X-ray with a wavelength of 0.6887 Å. NMR spectra were performed with the Bruker ARX400 (1H at 400 MHz). Photoluminescence (PL) was measured by FLS980 (Edinburgh Instruments Ltd) with an excitation at 470 nm. The in-situ photoluminescence (PL) measurement was carried out by FLS980 (Edinburgh Instruments Ltd) equipment. We spin-coated the Q-2D precursor solution onto ITO substrate, and detect the emission peak of the film for a growth period of 500 s, by using 470 nm excitation. The growth trend for the perovskite phase with different n was estimated from detecting the emission peak at 585 nm (n=2), 670 nm (n=4), and 780 nm (n=∞), respectively. The current density-voltage characteristics of photovoltaic devices were obtained using a Keithley 2400 source-measure unit. The photocurrent was measured under AM1.5G illumination at 100 mW/cm^2 under a Newport Thermal Oriel 91192 1000 W solar simulator. External quantum efficiencies were measured by an Enli Technology (Taiwan) EQE measurement system.

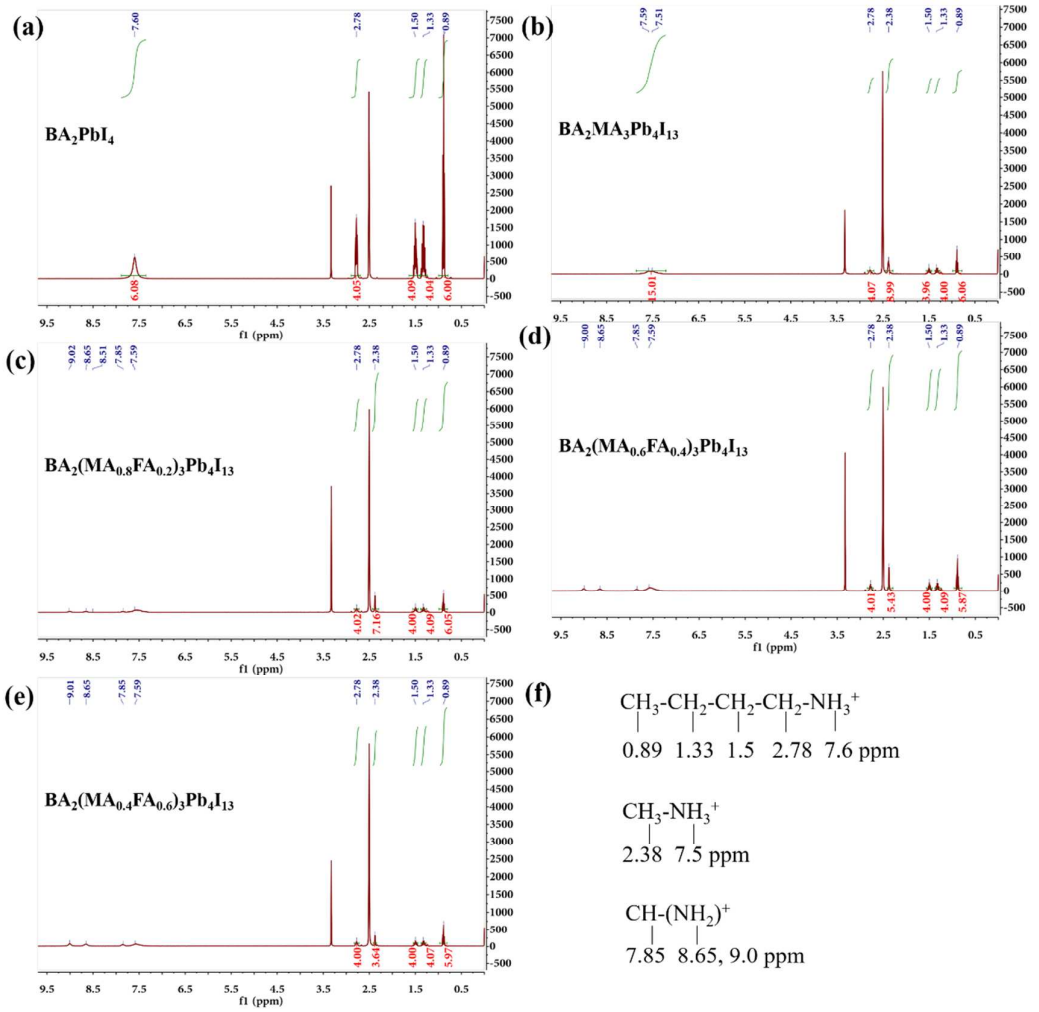

Figure S1. The HNMR spectra of (a) BA_2PbI_4; (b) $BA_2(MA)_3Pb_4I_{13}$; (c) $BA_2(MA_{0.8}FA_{0.2})_3Pb_4I_{13}$; (d) $BA_2(MA_{0.6}FA_{0.4})_3Pb_4I_{13}$; (e) $BA_2(MA_{0.4}FA_{0.6})_3Pb_4I_{13}$; (f) The chemical shift of the H from the different organic cations. The samples were scraped from the formed films.

The chemical shift located at 0 ppm、~2.51 ppm、~3.32 ppm represented $Si(CH_3)_4$, dimethyl sulfoxide-d6, H_2O, respectively. The chemical shift of the H from different organic cations was shown in Figure S1. We could readily acquire the actual ratio between MA and BA ratio by comparing the peak of CH_3 in MA^+ and CH_3 in BA^+. It should be noted that the peak of CH from FA (~7.85 ppm) is very close to the peak of NH_3 from MA^+ (7.5 ppm) and BA^+ (7.6 ppm), so we calculated the FA ratio based on the derived BA/MA ratio and a fixed ratio of BA/(MA+FA) at 2:3. We found that the actual *x* value in the final perovskite film is quite close to the ratio from the starting precursor material.

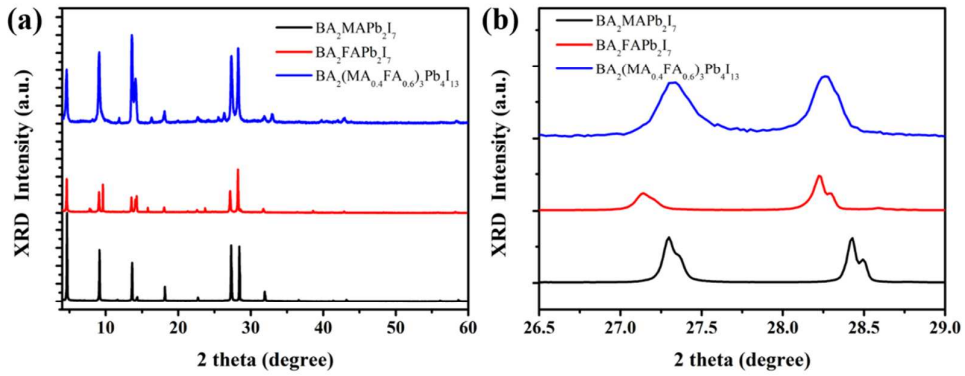

Figure S2 (a) XRD patterns of the $BA_2(MA)Pb_2I_7$, $BA_2(FA)Pb_2I_7$ and $BA_2(MA_{0.4}FA_{0.6})_3Pb_4I_{13}$ series Q-2D perovskite; (b) The magnify of XRD peak between 26.5°and 29°.

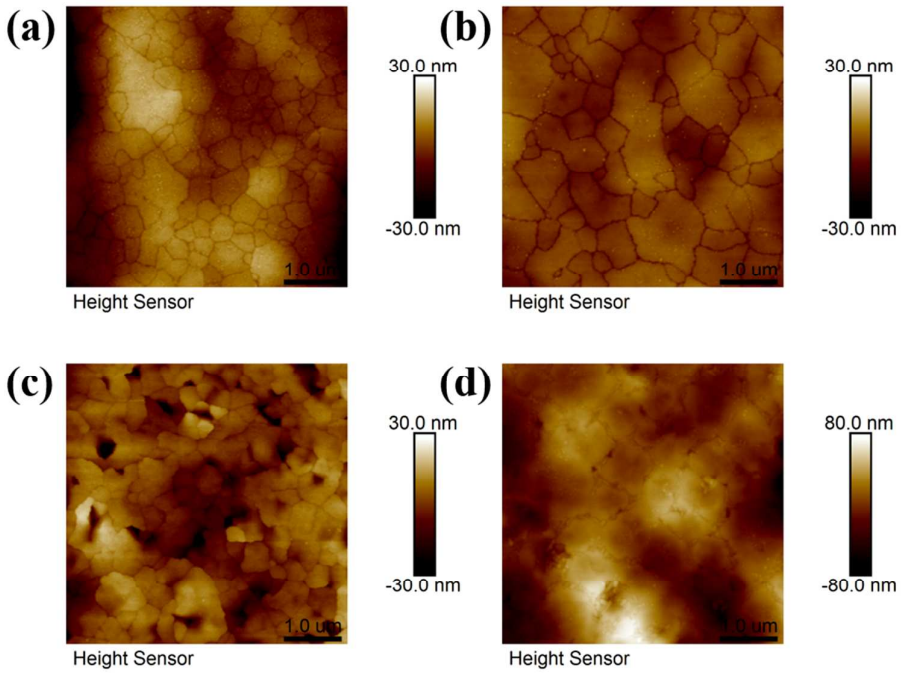

Figure S3. AFM images of $BA_2(MA_{1-x}FA_x)_3Pb_4I_{13}$ x=0, 0.2, 0.4, 0.6 films, respectively

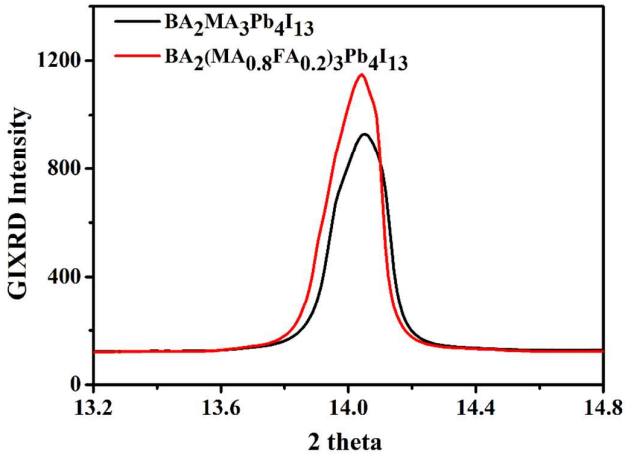

Figure S4. Integrated intensity plots of the GIWAXS patterns at 14.1° diffraction angle.

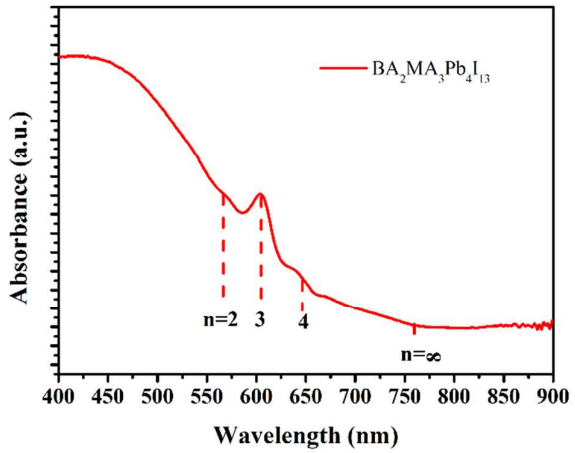

Figure S5. The absorption spectrum of $(BA)_2(MA)_3Pb_4I_{13}$ perovskite thin films.

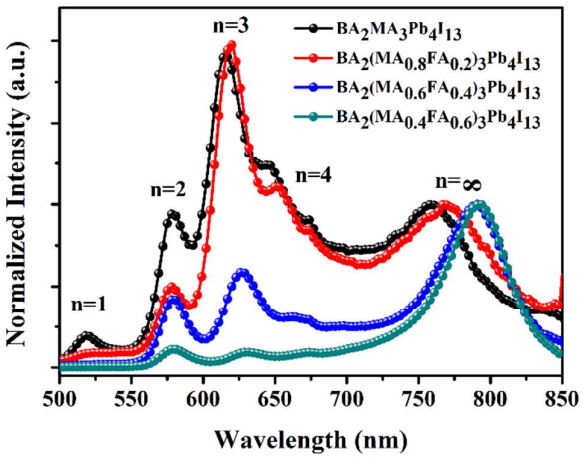

Figure S6. The steady-state PL spectra of the $BA_2(MA,FA)_3Pb_4I_{13}$ series Q-2D perovskite films from glass back side.

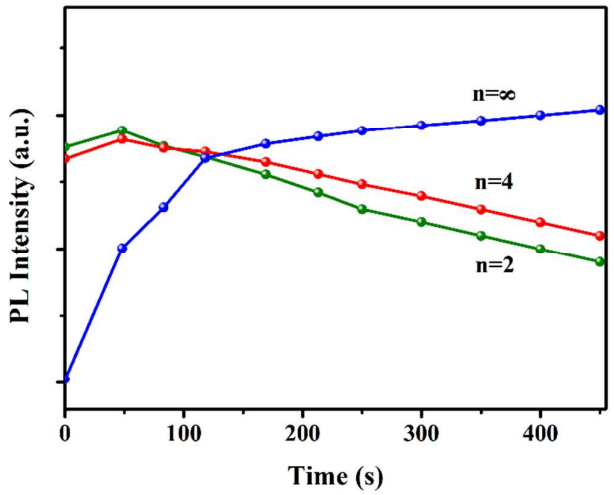

Figure S7. In-situ PL measurement for $BA_2(MA_{0.8}FA_{0.2})_3Pb_4I_{13}$ film by detecting the emission peak at 585 nm (n=2), 670 nm (n=4), and 780 (n=∞).

We carried out the in-situ PL to investigate the FA0.2 system (**Figure S7**), and the variation tendency is similar to FA0 system. However, the composition of n=∞ increased faster than FA0 system.

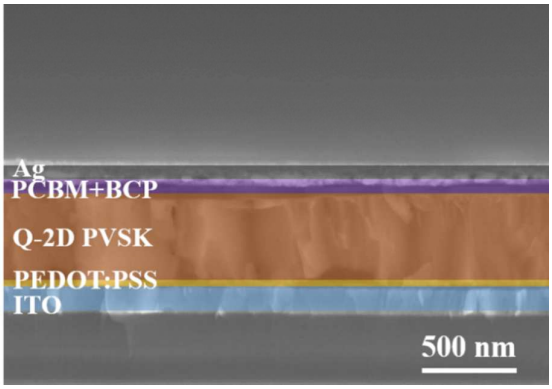

Figure S8. Cross sectional SEM image of the inverted planar perovskite solar cell.

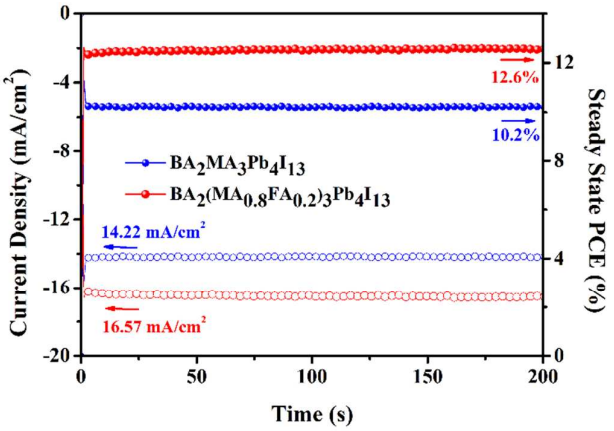

Figure S9. The steady-state PCE of the $BA_2(MA)_3Pb_4I_{13}$ (10.2% at a voltage of 0.72 V) and $BA_2(MA_{0.8}FA_{0.2})_3Pb_4I_{13}$ (12.6% at a voltage of 0.76 V) based perovskite solar cells.

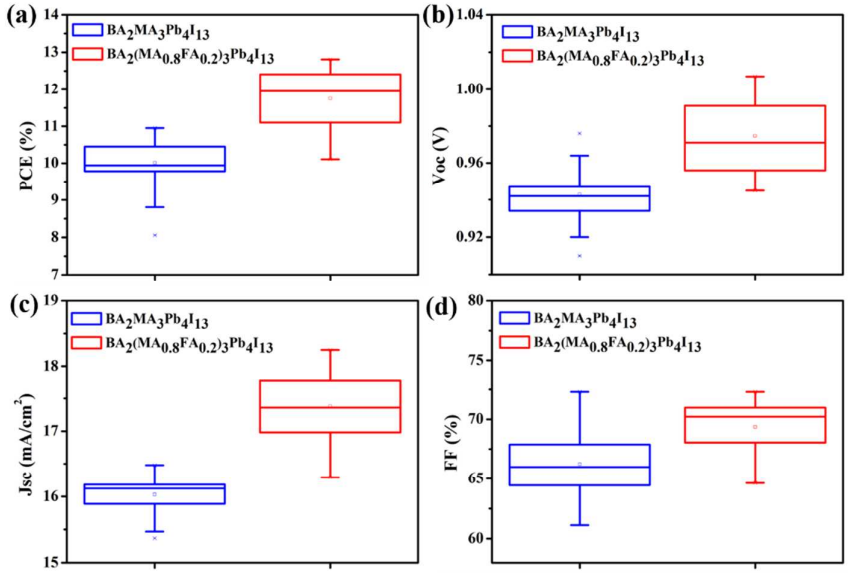

Figure S10. (a) PCE; (b) V_{oc}; (c) J_{sc}; (d) FF statistic distribution of $BA_2(MA)_3Pb_4I_{13}$ and $BA_2(MA_{0.8}FA_{0.2})_3Pb_4I_{13}$ based solar cells.

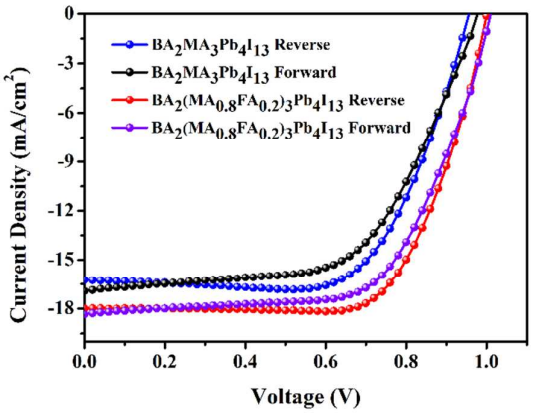

Figure S11. J-V characteristic for solar cell with reverse and forward scan directions.

Table S1. Hysteresis Factor Extracted from Data in **Figure 5b**

Using the Definition Provided in **Equation 1**.

Device	Scan Direction	Jsc at 0.8V_{oc} (mA/cm^2)	Hysteresis Index
$BA_2(MA)_3Pb_4I_{13}$	Reverse	13.07	0.149
	Forward	11.12	
$BA_2(MA_{0.8}FA_{0.2})_3Pb_4I_{13}$	Reverse	14.98	0.072
	Forward	13.90	

*__Equation 1.__ $HI=\frac{J_{RS\,(0.8Voc)}-J_{FS\,(0.8Voc)}}{J_{RS\,(0.8Voc)}} \times 100\%$

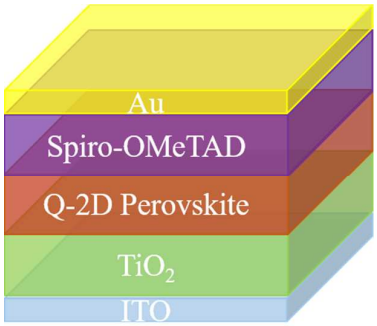

Figure S12. Scheme of a perovskite solar cell device for long term stability testing.

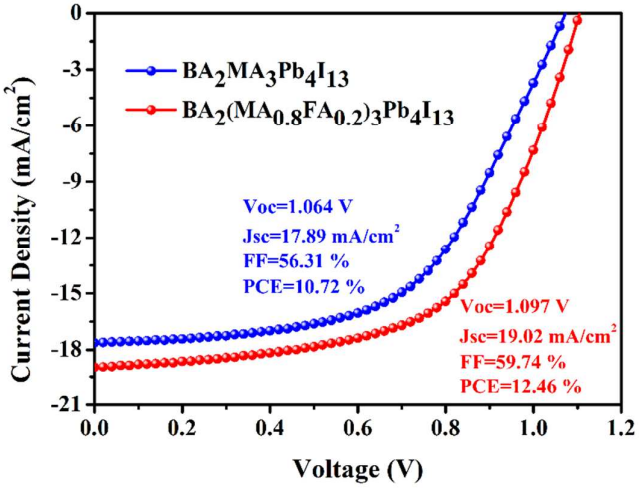

Figure S13. The J-V curve of $BA_2(MA)_3Pb_4I_{13}$ and $(BA)_2(MA_{0.8}FA_{0.2})_3Pb_4I_{13}$ based perovskite solar cells by adopting regular device structure (ITO/TiO_2/Perovskite/Spiro-OMeTAD/Au).

(1) Stoumpos, C. C.; Cao, D. H.; Clark, D. J.; Young, J.; Rondinelli, J. M.; Jang, J. I.; Hupp, J. T.; Kanatzidis, M. G. *Chem. Mater.* **2016**, *28*, 2852.